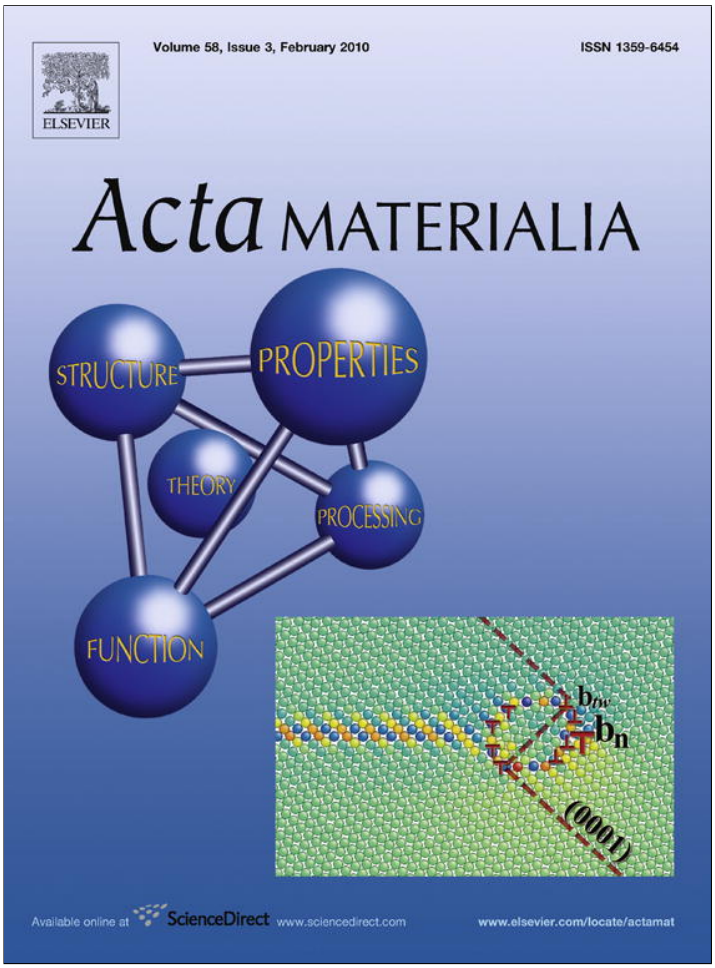

Available online at www.sciencedirect.com
ScienceDirect
Acta Materialia 58 (2010) 813–822
Acta MATERIALIA
www.elsevier.com/locate/actamat

The effects of grain grooves on grain boundary migration in nanofilms

Amy Novick-Cohen [a], Olga Zelekman-Smirin [a], Arkady Vilenkin [b,*]

[a] Department of Mathematics, Technion-IIT, Haifa 32000, Israel
[b] The Racah Institute of Physics, The Hebrew University of Jerusalem, Jerusalem 91904, Israel

Received 24 July 2009; received in revised form 15 September 2009; accepted 29 September 2009
Available online 31 October 2009

Abstract

Using numerical computations and asymptotic analysis, we study the effects of grain grooves on grain boundary migration in nanofilms, focusing for simplicity on axisymmetric bicrystals containing an embedded cylindrical grain located at the origin. We find there is a critical initial grain radius, R^*, such that if $R < R^*$, the grain at the origin shrinks and annihilates, and if $R > R^*$, groove growth during grain shrinkage leads to film break-up. The central cross-section of the grain boundary profile is seen to be parabolic, and an ordinary differential equation which depends on the tilt angle and the groove depth is seen to govern the location of the groove root. Near the annihilation–pinch-off transition, temporary stagnation occurs; thereafter, the shrinking grain accelerates rapidly, then disappears.

Keywords: Grain boundaries; Grain growth; Surface diffusion; Theory

1. Introduction

We consider a film which contains an axisymmetric grain located at the origin. The system evolves due to three-dimensional (3-D) motion by the mean curvature of the grain boundary coupled along a circular triple junction line to an external surface evolving via surface diffusion. Our system, which has no steady states, allows us to capture certain effects, such as stagnation, pinch-off and acceleration, which were not to be seen in earlier 2-D studies [1–3].

Stagnation of grain growth in polycrystalline films occurs during annealing when the average grain radius is greater than the film's thickness. See Ref. [4] for experimental observations of grain growth and stagnation in Al foils, as well as a discussion of other possible causes of stagnation. Proposed explanations for stagnation include solute drag, pinning of grain boundary by defects, and stagnation due to grain grooving resulting from surface diffusion. The present study explores this last conjecture within the framework of a simple but realistic 3-D model system. Mullins [5] suggested that in films with columnar structure, the groove root can act as an anchor, grains boundaries can take on a catenoidal-shaped surface with zero mean curvature, and grain boundary migration can come to a halt. Note that in Mullins' original 1958 paper [5], the notion of critical angle corresponded to the angle made by the grain boundary in steady 2-D traveling wave solutions. Although the configuration suggested by Mullins cannot be a steady state for the geometry which we consider, since our system has no steady states (see Appendix A), nevertheless it can be expected to evolve slowly. An approximate version of Mullins' idea was employed in Ref. [6] to model stagnation of grain growth in thin films. An algorithm was implemented in Ref. [6] which introduces the notion of a critical value for the in-plane curvature, such that if the inclination of the grain boundary to the external surface is equal to, or less than, the critical angle, then locally the grain boundary has the shape of a catenoid and should thus be stationary. Note that neither in Ref. [5] nor in Ref. [6] was any true 3-D problem considered. Nevertheless, the experimental data obtained in Ref. [7] fit the results of Ref. [6] fairly well. Catenoids and critical values of R_0/L, where L denotes half the initial thickness of the film, appear naturally in various related problems involving motion by mean curvature and surface diffusion, such as hole formation in thin films [8,9].

* Corresponding author. Tel.: +972 26584471; fax: +972 26512483.
E-mail address: vilenkin@vms.huji.ac.il (A. Vilenkin).

1359-6454/$36.00 © 2009 Acta Materialia Inc. Published by Elsevier Ltd. All rights reserved.
doi:10.1016/j.actamat.2009.09.059

It is well known that in polycrystalline nanofilms, grain grooves can often traverse the entire thickness of the film within a reasonable amount of time [10]. This can then lead to void formation, which can in turn lead to the agglomeration of the film. We point out that our present study is valid until the embedded grain annihilates or the grain groove penetrates the the thin film. If the groove root does penetrate the thin film, then the next stage of the dynamics would require an understanding of void or hole growth and stability. Modern experimental techniques now allow such phenomena to be observed; see e.g. Ref. [11] for experimental data on the kinetics of void formation and agglomeration in thin copper films, and related references. A theory for groove growth in flat stationary grain boundaries was proposed by Mullins [12]. A theoretical analysis of void formation in 2-D thin films during grain growth was presented in Ref. [13] for a one component system and in Ref. [14] for the growth of a stationary groove in a two component alloy system.

In the present paper we explore the transition between annihilation and break-up, focusing on accompanying features such as stagnation, grain boundary shape, and the acceleration which typically occurs just prior to grain annihilation. We summarize below our main results.

Our numerical results indicate that the dynamics of grain boundaries coupled with an external surface differ significantly from the dynamics of freely shrinking grains, and do not obey the postulated algorithm underlying the simulations in Ref. [6]. Since our system has no steady states, the embedded grain eventually either annihilates or leads to voiding along the grain boundary. Whether annihilation or voiding does in fact occur depends in our model on the film's thickness, the initial radius of the grain, the ratio of the grain boundary and the external surface energies, and on the kinetic coefficients: the grain boundary mobility and the surface diffusion coefficient. If the initial radius of the grain, R_0, is varied, while the other parameters are held fixed, we find there is a critical radius R^* such if $R_0 < R^*$, the grain at the origin shrinks and annihilates, and if $R_0 > R^*$, groove growth during grain shrinkage leads to film break-up; i.e. the groove depth reaches half the film thickness and the grain detaches from the film before the grain has time to annihilate. We find that while R^* depends linearly on L when $L \gg 1$, at small distinctly nanoscale values of L, the dependence is nonlinear. Although true stagnation is not possible for our 3-D problem, we observe significant delay of grain growth prior to pinch-off or grain annihilation when $R_0/R^* \gtrsim 1$. Hence it seems reasonable to consider R^* as a generalization of the notion of a critical in-plane curvature as discussed in Ref. [6]. It is not too surprising that the results of our investigations do not correspond too closely with the results reported in Ref. [6], because here, as in Ref. [15], the dynamics coupling the time evolution of the grain boundary and the external surfaces are truly 3-D. Our numerical simulations exhibit acceleration of the rate of shrinkage of the grain just prior to annihilation. Jerky motion [5] was not observed.

The paper also contains an asymptotic analysis of the mathematical model, based on the assumption that m and L/R_0 are small, where m denotes the ratio of grain boundary to external surface energies. To leading order, the coupled motion of the exterior surface and grain boundary can be stated in terms of a partial differential equation (PDE) for the exterior surface which couples via the boundary data with an ordinary differential equation (ODE) for $R(t)$, the distance of the groove root to the origin,

$$R_t = A\left[\frac{r_u^*}{u^*} - \frac{1}{R}\right], \tag{1.1}$$

where r_u^*, u^* denote the tilt angle and the thickness of the film at the groove root, respectively. The prediction (1.1) was strongly confirmed by our numerical calculations. The grain boundary is shown to have a parabolic profile to leading order, which was also robustly confirmed by our numerical calculations. If the additional assumption is made that R_0 is quite large and $mR_0/L = \mathcal{O}(1)$, then a radial variant of Mullins' equation for thermal grooving [5,16] is obtained, and break-up can be expected. If R_0 is quite large, but nevertheless $mR_0/L = \mathcal{O}(m^\alpha)$ where $0 < \alpha < 1$, then to leading order the motion in the vicinity of the groove root is governed by a quasi-steady traveling wave solution whose velocity is controlled by (1.1) with $r_u^*/u^* = m/6L$. It is interesting to note that the term $m/(6L)$ corresponds to the small angle approximation which was proposed by Mullins [5] and implemented by Dunn [17] for the out-of-plane component of the mean curvature.

2. The mathematical model

A description of the physical processes which influence the coupled motion of groove roots and exterior surfaces can be found in Mullins' 1958 paper [5]. Although the discussion given there is limited to the linear regime and the coupling of the grain boundary motion is not fully considered, the discussion given there can be generalized to encompass nonlinear effects and the motion of the grain boundary [1,2,15]. This model is formulated below in the context of a thin film bicrystalline specimen with an axisymmetric geometry and with reflection symmetry about its midplane. For simplicity, as in Mullins [5], the possible effects of anisotropy have been neglected, as have possible nonequilibrium or kinetic effects on the balance of mechanical forces, elasticity effects and defect effects. These model equations provide, in a sense, a simplest possible framework in which to consider coupled grain boundary and external surface motions, and thus are noteworthy for the rich phenomena that they nevertheless exhibit.

The grain boundary is assumed to evolve by mean curvature, $V = A\kappa$, and the exterior surface is assumed to evolve by surface diffusion, $V = -B\triangle_s\kappa$. Here V and κ denote the normal velocity and the mean curvature of the grain boundary and of the exterior surface, respectively, A, B are kinetic coefficients, and $\triangle_s$ denotes the surface Laplacian. Along the groove root, the boundary conditions are assumed to include (i) a "persistence condition" stating that grain boundary and

the exterior surface remain attached; (ii) a balance of mechanical forces (Young's law): $\frac{1}{\sin(\theta_{\text{left}})} = \frac{1}{\sin(\theta_{\text{right}})} = \frac{m}{\sin(\theta_{\text{groove}})}$, where $\theta_{\text{left}}, \theta_{\text{right}}$ are the angles between the exterior surface and the grain boundary, θ_{groove} is the dihedral angle at the groove root, and $m = \gamma_{\text{grain boundary}}/\gamma_{\text{exterior surface}}$, the ratio of the surface free energies of the exterior surface and the grain boundary; (iii) continuity of the chemical potential, $\kappa^+ = \kappa^-$, where $\kappa^\pm$ denotes the mean curvature evaluated on either side of the groove root; and (iv) balance of mass flux, $[\vec{n}\cdot\nabla_s\kappa]^+ = [\vec{n}\cdot\nabla_s\kappa]^-$, where $[\vec{n}\cdot\nabla_s\kappa]^\pm$ denotes the gradient of the mean curvature on either side of the groove root. Far away from the grain located at the origin, the original bicrystal configuration is assumed to be preserved. These equations constitute a reasonable mathematical model until the "geometry" of the model breaks down, due to annihilation of the grain at the origin or to break-up of the film.

Our governing equations contain three physical parameters, A, B, m, whose dimensions are given by $[A] = X^2/T, [B] = X^4/T, [m] = 1$, as well as two geometric parameters, R_0, L, whose dimensions are given by $[R_0] = X, [L] = X$, where R_0 denotes the initial radius of the grain embedded at the origin and L denotes half of the unperturbed thickness of the thin nanofilm. We use A and B to define typical length and time scales, $\overline{T} = B/A^2$, $\overline{X} = \sqrt{B/A}$, and formulate our mathematical model in terms of the dimensionless parameters $m, R_0\ (= R_0/\overline{X}), L\ (= L/\overline{X})$, and the dimensionless (scaled) variables $r = r(u,t), h = (r,t), u^* = u^*(t)$, and $R = R(t)$, as defined in Fig. 1.

In terms of these parameters and variables, motion by mean curvature and motion by surface diffusion may be stated, respectively, as

$$r_t = \frac{r_{uu}}{1+r_u^2} - \frac{1}{r}, \quad 0 < u < u^*(t), \tag{2.2}$$

and

$$h_t = -\frac{1}{r}\frac{\partial}{\partial r}\left[\frac{rk_r}{\sqrt{1+h_r^2}}\right], \quad 0 < r < \infty,\ r \neq R(t), \tag{2.3}$$

where

$$k = \frac{1}{r}\frac{\partial}{\partial r}\left[\frac{rh_r}{\sqrt{1+h_r^2}}\right]. \tag{2.4}$$

Eqs. (2.2)–(2.4), as well as the boundary conditions (2.5)–(2.13) prescribed below, should be valid for $0 < t < T$, where T denotes the (scaled) time at which the model breaks down due to annihilation of the grain at the origin or pinch-off due to groove root penetration of the film.

Along the grain groove, (i) the persistence condition may be stated as

$$u^*(t) = L + h(R(t)^\pm, t), \quad r(u^*(t), t) = R(t), \tag{2.5}$$

$$h(R(t)^+, t) = h(R(t)^-, t), \tag{2.6}$$

(ii) Young's law implies that

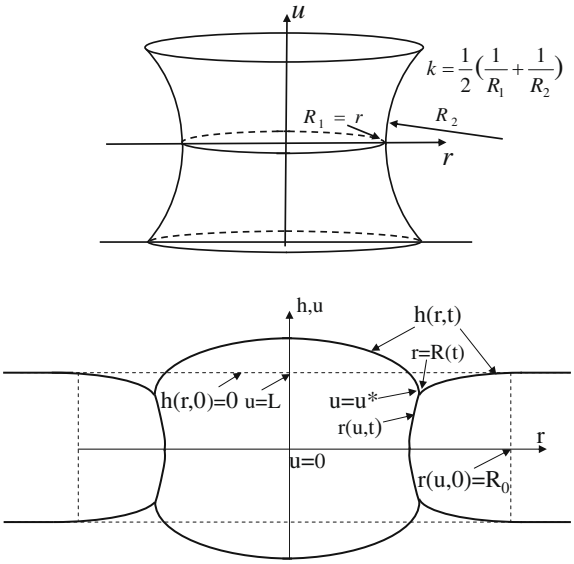

Fig. 1. The upper panel shows the curvatures along the grain boundary surface. The lower panel indicates the definition of the variables in the central cross-section.

$$\arctan(h_r(R(t)^+, t)) - \arctan(h_r(R(t)^-, t)) = 2\arcsin(m/2), \tag{2.7}$$

$$\arctan(h_r(R(t)^+, t)) + \arctan(h_r(R(t)^-, t)) + 2\arctan(r_u(u^*(t), t)) = 0, \tag{2.8}$$

(iii) continuity of the chemical potential gives that

$$k(R(t)^+, t) = k(R(t)^-, t), \tag{2.9}$$

and (iv) balance of mass flux may be stated as

$$\frac{k_r}{\sqrt{1+h_r^2}}\Big|_{(R(t)^+,t)} = \frac{k_r}{\sqrt{1+h_r^2}}\Big|_{(R(t)^-,t)}. \tag{2.10}$$

At the origin, axisymmetry implies that

$$h_r(0,t) = 0, \quad k_r(0,t) = 0, \tag{2.11}$$

and at $u = 0$, symmetry of the thin film with respect to its midplane implies that

$$r_u(0,t) = 0. \tag{2.12}$$

And finally, the far-field conditions may be written as

$$h(\infty, t) = k(\infty, t) = 0. \tag{2.13}$$

Eqs. (2.2)–(2.13) are to be solved in conjunction with the initial conditions

$$r(u,0) = R_0, \quad 0 < u < L, \quad h(r,0) = 0, \quad 0 < r < \infty. \tag{2.14}$$

3. Numerics

3.1. Methodology

Suppose that the solution is known up to time t for some $t > 0$, and suppose that past values of $R(t)$ are used to approximate $R(t + \triangle t)$ for some $\triangle t > 0$. Taking $R(t + \triangle t)$ to be now known, the equations in problem

(2.2)–(2.14) can be used to approximate $h(r, t+\triangle t)$ and then $r(u, t+\triangle t)$. This can be accomplished by first solving a "surface problem" for $h(r, t+\triangle t)$ using an implicit finite-difference scheme based on the equations for surface diffusion, (2.3) and (2.4), and the boundary conditions which depend on h and k only: (2.6) and (2.7), (2.9), (2.10), (2.11) and (2.13). Having approximated $h(r, t+\triangle t)$, an approximation for $u^*(t+\triangle t) = L + h(R(t+\triangle t), t+\triangle t)$ which appears in (2.5) is implied. The value of $u^*(t+\triangle t)$, the boundary condition (2.12) and the equation for grain boundary motion (2.2), together constitute a "grain boundary problem" whose solution via an implicit finite-difference scheme gives an estimate of $r(u, t+\triangle t), 0 < u < u^*(t+\triangle t)$. By now, all of the equations and boundary conditions in problem (2.2)–(2.14) have been used, except for the second condition implied by Young's law, (2.8), which connects $h_r(R(t+\triangle t), t+\triangle t)$ and $r_u(u^*, t+\triangle t)$. This last condition can be used to correct the approximation for $R(t+\triangle t)$. This process can be iterated until sufficient accuracy is achieved. The initial conditions have been taken in accordance with (2.7), (2.8) and (2.14), in that Young's law has been imposed at the groove root on the finest finite-difference scale for the sake of compatibility.

3.2. Physical conclusions indicated by our numerical results

Our numerical results clearly indicate the appearance of a transition between annihilation and break-up (see Fig. 2). Recall, however, that when $m = 0$, which corresponds to the case of a "freely moving grain boundary," annihilation is always indicated, because no groove root forms in this case. Roughly speaking the transition can be described in terms of the "aspect ratio" $a = R_0/L$. There appears to be a critical aspect ratio, a_c, such that for $a < a_c$, the grain at the origin is "sufficiently small" so that annihilation ensues, and if $a > a_c$, the thin film is "sufficiently thin" such that break-up occurs. The critical aspect ratio, a_c, can be seen to decrease as m increases, which corresponds to an increase in the relative energy of the grain boundary surface, and hence in the tendency towards break-up. Note that while for $L \gg 1$ a_c is independent of L, when $L \approx 0.1 - 0.5$ or smaller, a_c can be seen to depend nonlinearly on L; recalling that $\overline{X} = \sqrt{B/A} \approx 4 \times 10^{-9}$ m has been used as the scaling length, we see that a cross-over from linear to nonlinear behavior of the annihilation–break-up transition occurs when the film thickness reaches the nanoscale. The grain radius $R(t)$ as a function of time is portrayed in Fig. 3 for $m = 0.1$ and $L = 1$. Where $R_0 = 1$ in Fig. 3, annihilation occurs and $R(t)$ can be seen to closely approximate the theoretical prediction, $R(t) = \sqrt{R_0^2 - 2t}$, which holds for the $m = 0$ case of a "free moving grain boundary." Where $R_0 = 112.5$ and 114.05 in Fig. 3, a transition between annihilation and break-up can be seen to occur roughly at $R_0 = 112.75$. The behavior of the grain radius as a function of time can be seen to be quite similar for values of R_0 just above and below the transitional value, with a long period of relative stagnation appearing in both cases. The overall rate of decrease in size of the grain radius is much slower for both these cases than for the case $m = 0$ of the freely moving grain boundary.

The depth of the groove root as a function of time on two different time scales can be seen in Fig. 4. Some oscil-

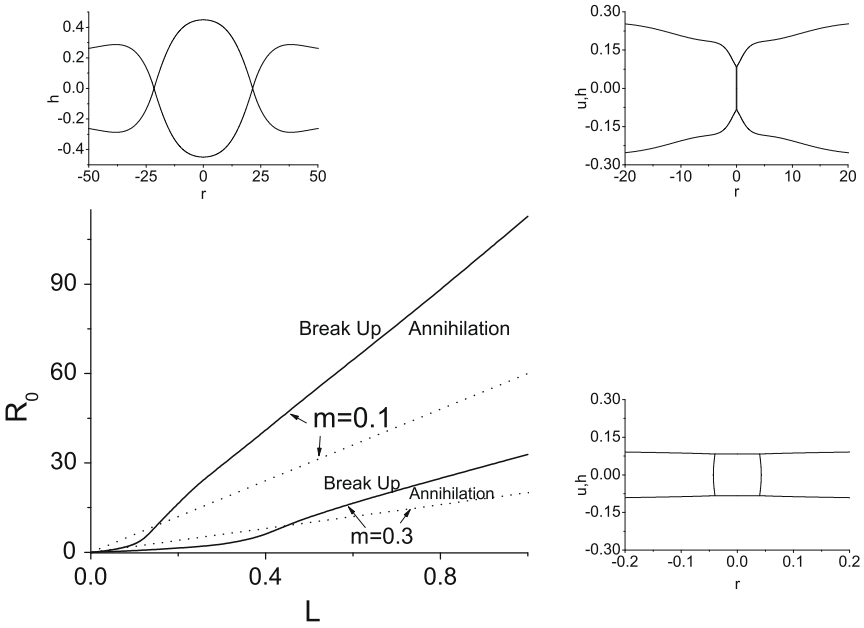

Fig. 2. The graph in the lower left panel indicates the transition between annihilation and break-up. The solid lines corresponds to our computations, the dotted lines correspond to Mullins' criterion for stagnation: $L/R_0 = m/6$, see Refs. [5,17]. Upper left panel: thin film break-up. Here $m = 0.1, L = 0.25, R_0 = 30$, and $t = 1761$. Right panels: grain annihilation. The same plot is given on two scales. Here $m = 0.1, L = 0.25, R_0 = 20$, and $t = 773.6$.

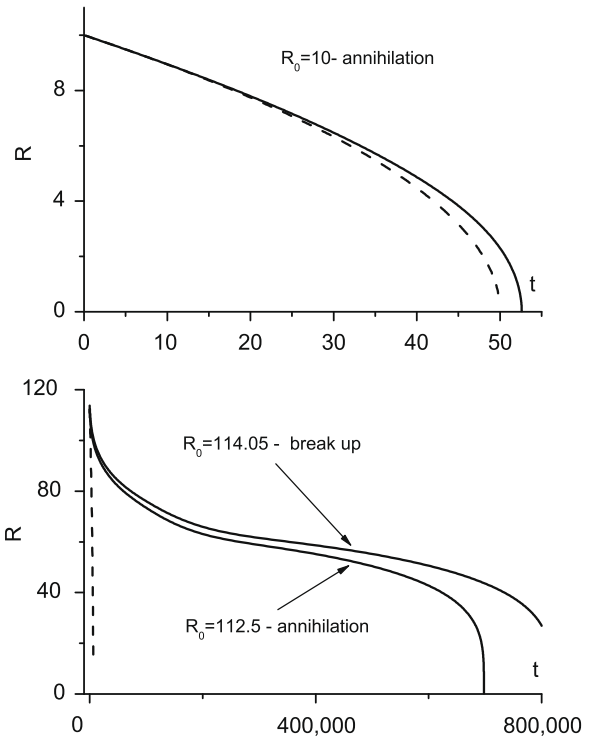

Fig. 3. The grain radius $R(t)$ as a function of time. Here $m = 0.1, L = 1$, and the annihilation–break-up transition occurs at $R_0 = 112.7$. The dashed line indicates $R(t)$ vs. t for a freely moving grain boundary ($m = 0$).

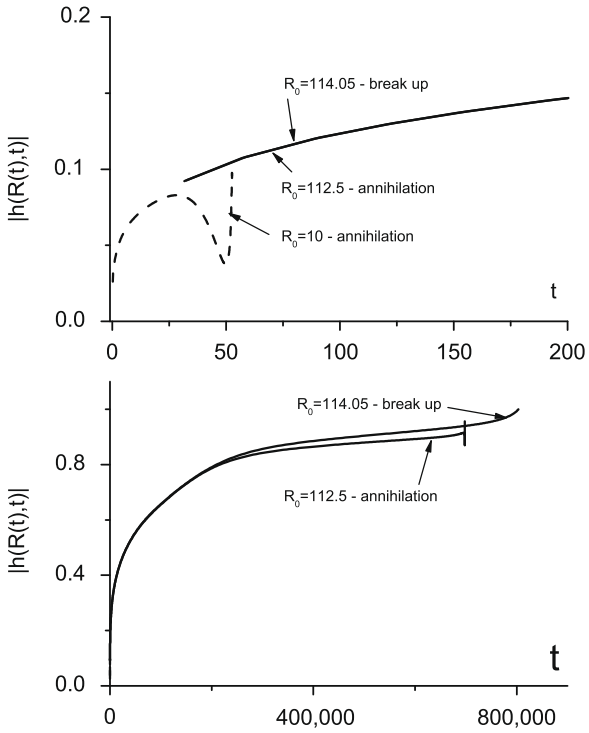

Fig. 4. The depth of the groove root as a function of time on two different time scales. Here $m = 0.1, L = 1$, and the annihilation–break-up transition occurs at $R_0 = 112.75$.

lations can be seen just prior to annihilation when R_0 is sufficiently small. We observed similar behavior during the shrinking of a spherical segment shaped grain attached to an external surface [15]. Note, however, that for R_0 just above and below its critical value, the time dependence in both two cases appears quite similar throughout the evolution of the system.

The inclination of the grain boundary at the groove root as a function of time is portrayed in Fig. 5. Just prior to annihilation, the inclination of the grain boundary at the groove root can be seen to change its direction. Until then, and up to and during break-up, $r_u(u^*) > 0$, which implies that the principal curvatures here are of the opposite sign, and corresponds to the observed stagnation.

In terms of the shape of the grain boundary, as break-up is approached, the grain boundary maintains a roughly self-similar parabolic shape while loosing height, and the direction of the grain boundary inclination does not change. See Figs. 3–6. As annihilation is approached, we see from Figs. 5 and 6 that here also the grain boundary appears to maintain a roughly self-similar parabolic profile, though just prior to annihilation, the grain boundary inclination changes sign. This change in the sign of the inclination of the grain boundary is indicative of a change in sign of one of the principle curvatures, and confirms the decrease in the height of the exterior surface of the shrinking grain (see Fig. 6), and subsequent acceleration seen in Fig. 5. The parabolicity of the grain boundary profile is discussed further in Section 4.

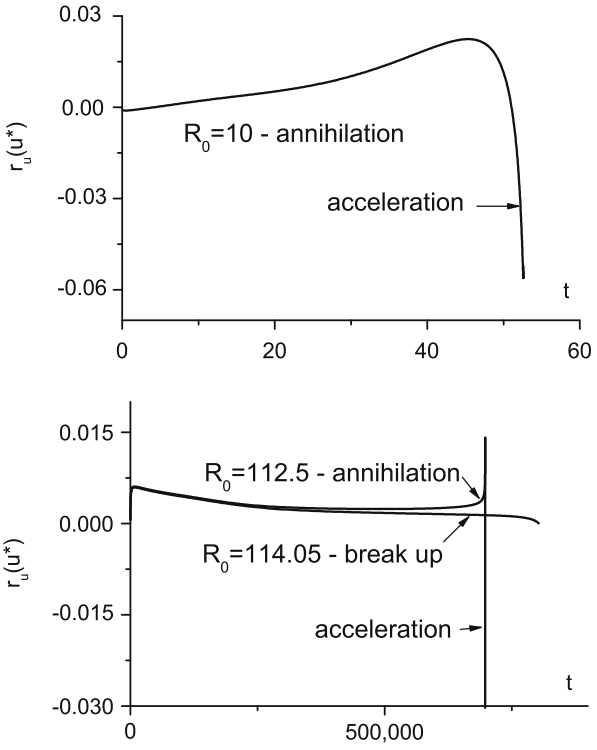

Fig. 5. The inclination of the grain boundary at the groove root as a function of time. Here $m = 0.1, L = 1$, and the annihilation–break-up transition occurs at $R_0 = 112.75$.

In Figs. 7 and 8, we verify our asymptotic predictions for the motion of the grain boundary which are derived

in Section 4. Note in particular that the fit of the numerical data with our asymptotic results is quite good until quite close to annihilation.

4. Asymptotic analysis

In this section, we assume that m and λm are small parameters, where $\lambda = L/(mR_0)$. We reformulate the problem (2.2)–(2.14) into a fixed domain by introducing the variables $p = r/R(t)$ and $s = u/u^*(t)$, and we also set

$$H(p,t) = \frac{R_0}{R(t)L} h(r,t)|_{r=R(t)p}, \quad K(p,t) = \frac{R_0 R(t)}{L} k(r,t)|_{r=R(t)p}, \tag{4.15}$$

$$\rho(s,t) = \frac{1}{u^*(t) r_u(u^*(t))} \{r(u,t) - R(t)\}|_{u=u^*(t)s}. \tag{4.16}$$

After some computations, for $0 < t < T$ we obtain

$$\frac{1}{r_u^* u^*} R_t + \frac{(r_u^* u^*)_t}{r_u^* u^*} \rho - \frac{u_t^*}{u^*} s\rho_s + \rho_t = \frac{1}{r_u^* (u^*)^2} \left[\frac{r_u^* \rho_{ss}}{1 + (r_u^*)^2 \rho_s^2} - \frac{u^*}{R + r_u^* u^* \rho} \right], \quad 0 < s < 1, \tag{4.17}$$

where $r_u^* := r_u(u^*(t), t)$,

$$\frac{R_t}{R}(H - pH_p) + H_t = -\frac{1}{R^4 p} \frac{\partial}{\partial p} \left[\frac{pK_p}{\sqrt{1 + \lambda^2 m^2 H_p^2}} \right], \quad 0 < p < \infty, \ p \neq 1, \tag{4.18}$$

$$K = \frac{1}{p} \frac{\partial}{\partial p} \left[\frac{pH_p}{\sqrt{1 + \lambda^2 m^2 H_p^2}} \right], \tag{4.19}$$

to be solved together with the following boundary and initial conditions

$$u^*(t)/L = 1 + (R(t)/R_0) H(1^{\pm}, t), \tag{4.20}$$

$$r_u^*(t) = -\frac{1}{2} \tan\left[\arctan(\lambda m H_p(1^+, t)) + \arctan(\lambda m H_p(1^-, t)) \right], \tag{4.21}$$

$$\arctan(\lambda m H_p(1^+, t)) - \arctan(\lambda m H_p(1^-, t)) = 2 \arcsin(m/2), \tag{4.22}$$

$$\rho(1,t) = 0, \ \ \rho_s(1,t) = 1, \tag{4.23}$$

$$H(1^+, t) = H(1^-, t), \tag{4.24}$$

$$K(1^+, t) = K(1^-, t), \ \ \frac{K_p}{\sqrt{1 + \lambda^2 m^2 H_p^2}}|_{(1^+,t)} = \frac{K_p}{\sqrt{1 + \lambda^2 m^2 H_p^2}}|_{(1^-,t)}. \tag{4.25}$$

$$H_p(0,t) = 0, \ \ K_p(0,t) = 0, \ \ \rho_s(0,t) = 0, \tag{4.26}$$

$$H(\infty, t) = K(\infty, t) = 0, \tag{4.27}$$

$$R(0) = R_0, \ \ u^*(0) = L, \ \ r_u^*(0) = 0, \tag{4.28}$$

$$\rho(s,0) = 0, \ \ 0 < s < 1, \ \ H(p,0) = 0, \ \ 0 < p < \infty. \tag{4.29}$$

We shall identify the leading order approximation to (4.17)–(4.29), assuming that H, K, ρ, p, s, and t have all been appropriately scaled so that H, K, ρ, and time derivatives are $\mathcal{O}(1)$ or smaller. From consideration of (4.21) and (4.22), we get that $r_u^*(t) = \mathcal{O}((1 + \lambda)m)$. From (4.20) and (4.28), we see that it is reasonable to assume that $u^*(t) = \mathcal{O}(L)$ and $R(t) = \mathcal{O}(R_0)$. From the estimates outlined above, we may conclude that $\lambda m H_p \ll 1$, $r_u^* \rho_s \ll 1$, $r_u^* u^* \rho \ll R$, and that $(r_u^* u^*)^{-1} R_t$ is far larger that the other terms on the right-hand side of (4.17). Thus, to leading order, for $0 < t < T$,

$$R_t = \left[\frac{r_u^*}{u^*} \rho_{ss} - \frac{1}{R} \right], \quad 0 < s < 1, \tag{4.30}$$

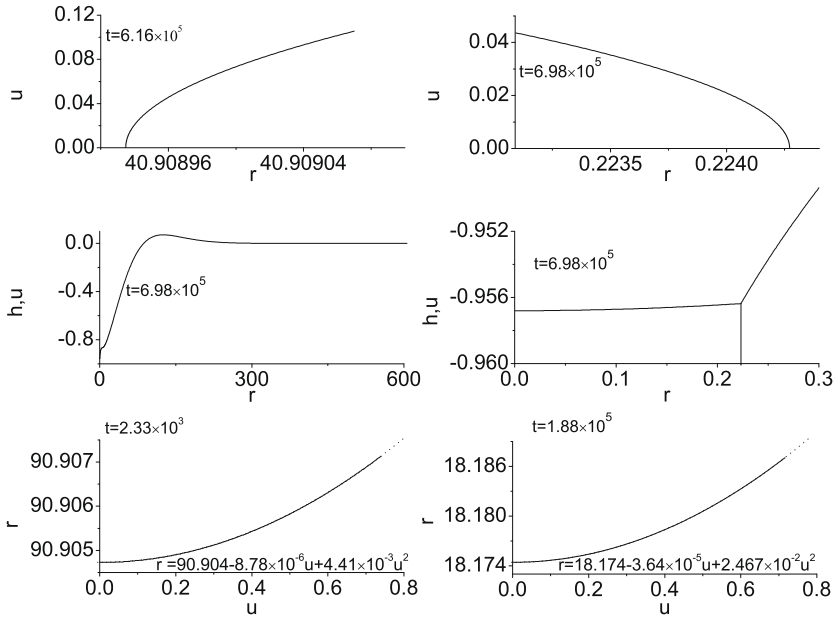

Fig. 6. The grain boundary and external surface profiles for $R_0 < R_c$. Upper panels: the shape of the grain boundary during annihilation. Here $m = 0.1, L = 1, R_0 = 112.75$, with the critical value for R_0 being given by $R_0 = 112.75$. Middle panels: the exterior surface and the grain boundary just before annihilation for the same parameters as above on different scales. Lower panels: the shape of the grain boundary can be seen to be quite close to parabolic (dotted line) throughout the numerical simulation. The parameters used here are $m = 0.1$, $R_0 = 100$, and $L = 1$.

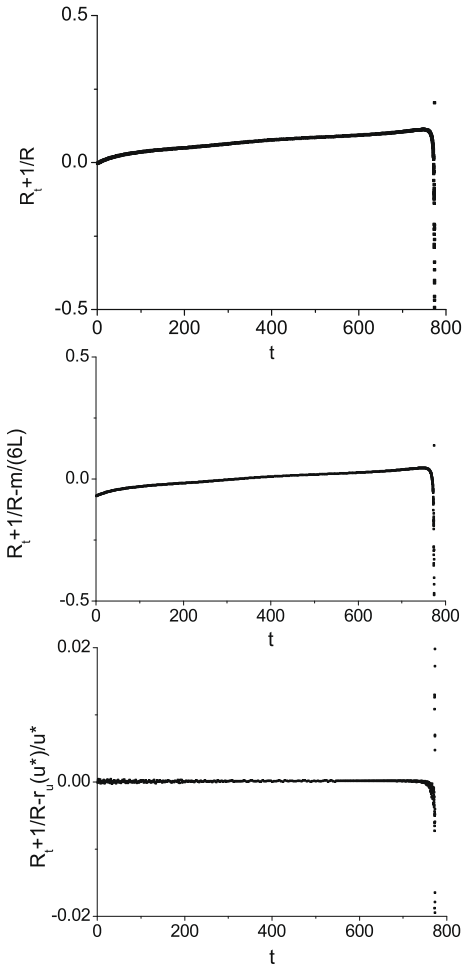

Fig. 7. Top panel: the deviation of the speed of the grain boundary from that of a freely moving grain boundary. Middle panel: the deviation of the speed of the grain boundary from the asymptotic prediction, (4.53). Lower panel: the deviation of the speed of the grain boundary from the asymptotic prediction, (4.33). The parameters used here are $m = 0.1, R_0 = 20$, and $L = 0.25$.

$$\frac{R_t}{R}(H - pH_p) + H_\tau = -\frac{1}{R^4 p}\frac{\partial}{\partial p}[pK_p],$$

$$K = \frac{1}{p}\frac{\partial}{\partial p}[pH_p], 0 < p < \infty,\ p \neq 1,$$

and along the grain groove,

$$u^*(t)/L = 1 + (R(t)/R_0)H(1^\pm, t),$$

$$r_u^*(t) = -(\lambda m/2)[H_p(1^+, t) + H_p(1^-, t)], \tag{4.31}$$

$$\rho_s(0,t) = \rho(1,t) = 0, \quad \rho_s(1,t) = 1, \tag{4.32}$$

$$H(1^+, t) = H(1^-, t), \quad H_p(1^+, t) - H_p(1^-, t) = 1/\lambda,$$

$$K(1^+, t) = K(1^-, t), \quad K_p(1^+, t) = K_p(1^-, t),$$

with the additional conditions

$$R(0) = R_0, \quad u^*(0) = L, \quad r_u^*(0) = 0, \quad \rho(s,0) = 0, \quad 0 < s < 1,$$

$$H_p(0,t) = K_p(0,t) = \rho_s(0,t) = 0, \quad H(\infty,t) = K(\infty,t) = 0,$$

$$H(p,0) = 0, \quad 0 < p < \infty.$$

Integrating (4.30) with respect to s over the interval [0, 1] and using (4.32),

$$R_t = \left[\frac{r_u^*}{u^*} - \frac{1}{R}\right]. \tag{4.33}$$

Eq. (4.33) may be understood as expressing motion by mean curvature, where both components of the principle curvatures are taken into account. See Fig. 7. Subtracting (4.33) from (4.30) and assuming r_u^*/u^* to be non-vanishing for $0 < t < T$,

$$\rho_{ss} - 1 = 0, \quad 0 < s < 1. \tag{4.34}$$

From (4.34) and (4.32), it follows that

$$\rho(s) = \frac{1}{2}(s^2 - 1), \quad 0 < s < 1, \tag{4.35}$$

which predicts the grain boundary profile to be parabolic, as seen in Fig. 6.

To leading order, for $0 < t < T$, we have obtained the following reduced description for the coupled dynamics

$$\frac{R_t}{R}(H - pH_p) + H_t = -\frac{1}{R^4 p}\frac{\partial}{\partial p}[pK_p],$$

$$K = \frac{1}{p}\frac{\partial}{\partial p}[pH_p], \quad 0 < p < \infty,\ p \neq 1, \tag{4.36}$$

$$R_t = \left[\frac{r_u^*}{u^*} - \frac{1}{R}\right], \tag{4.37}$$

$$H(1^+, t) = H(1^-, t), \quad H_p(1^+, t) - H_p(1^-, t) = 1/\lambda, \tag{4.38}$$

$$K(1^+, t) = K(1^-, t), \quad K_p(1^+, t) = K_p(1^-, t), \tag{4.39}$$

$$H_p(0,t) = K_p(0,t) = H(\infty,t) = K(\infty,t) = 0, \tag{4.40}$$

$$R(0) = R_0, \quad H(p,0) = 0, \quad 0 < p < \infty, \tag{4.41}$$

$$u^*(t)/L = 1 + (R(t)/R_0)H(1^\pm, t), \tag{4.42}$$

$$r_u^*(t) = -(\lambda m/2)[H_p(1^+, t) + H_p(1^-, t)]. \tag{4.43}$$

Thus, to leading order, the dynamics are given in terms a PDE for $H(p,t)$, which describes the exterior surface, coupled with an ODE for $R(t)$, the distance of the groove root from the radial axis of symmetry of the system.

The system (4.36)–(4.43) contains three dimensionless parameters, m, R_0, and L, with λ being determined by $\lambda = L/(mR_0)$. There are two asymptotic limits of (4.36)–(4.41), (4.43) which can be readily considered.

(I) Suppose that R_0 is quite large, and that $1/\lambda = mR_0/L = \mathcal{O}(1)$. By (4.38), (4.43), $r_u^*(t) = \mathcal{O}((1+\lambda)m)$, and at least initially $u^*(t) \approx L$ and $R(t) \approx R_0$. Hence (4.37) implies that $R_t \approx 0$. Returning to (4.36)–(4.43), we now see that to leading order the evolution should be given by

$$H_t = -\frac{1}{R^4 p}\frac{\partial}{\partial p}[pK_p], \quad K = \frac{1}{p}\frac{\partial}{\partial p}[pH_p], \quad 0 < p < \infty,\ p \neq 1,$$

$$H(1^+, t) = H(1^-, t), \quad H_p(1^+, t) - H_p(1^-, t) = 1/\lambda,$$

$$K(1^+, t) = K(1^-, t), \quad K_p(1^+, t) = K_p(1^-, t),$$

$$H_p(0,t) = K_p(0,t) = H(\infty,t) = K(\infty,t) = 0,$$

$$H(p,0) = 0, \quad 0 < p < \infty,$$

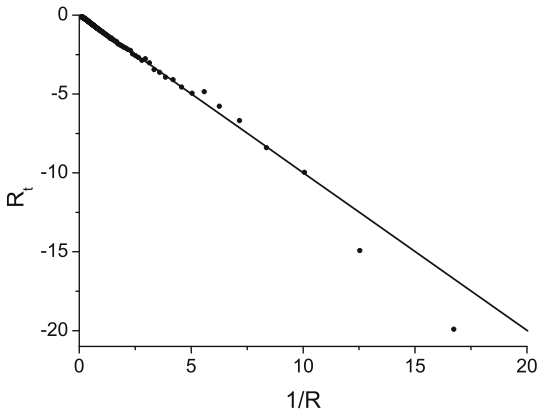

Fig. 8. Comparison of numerical data (scattered dots) with our asymptotic predictions (solid line) which correspond to the solution of $R_t = m/(6L) - 1/R$. The parameters used here are $m = 0.1$, $R_0 = 10$, and $L = 1$.

with $R(t) \approx R_0$. This system can be considered as a radial variant of Mullins' equation for thermal grooving [5,16], and break-up should be expected.

(II) Suppose that R_0 is large, but not too large in that we set $\lambda = L/mR_0 = m^{-\alpha}$ where $0 < \alpha < 1$. Then, again (4.38), (4.43) imply that $r_u^*(t) = \mathcal{O}((1+\lambda)m)$, and that at least initially, $u^*(t) = \mathcal{O}(L)$. Hence (4.37) implies that $R(t)$ will commence shrinking, largely uninfluenced by the evolution of $H(p,t)$. Under these circumstances, $H_t(t,p)$ in turn can be expected to be small, and $H(p,t)$ can be expected to vary primarily in the close proximity of the groove root.

It is possible to understand the structure of this solution by describing it in terms of an "inner" or "corner" solution designed to capture the behavior of the solution in the proximity of the groove root, and this "inner" or "corner" solution must "matched up" with "outer" solutions describing the behavior of $H(p,t)$ away from the groove root. In order to obtain a description of the "inner" or "corner" solution, which is expected to vary only slightly and only over a small spatial interval, we introduce the variables

$$q = (p-1)/\delta_1, \quad y = \frac{1}{\delta_2} H(p,t)|_{p=1+\delta_1 q}, \tag{4.44}$$

and where δ_1, δ_1 are small parameters which are set so that $\delta_2/\delta_1 = 1/\lambda$ and $\delta_1 = R_0^{-2/3}$.

In terms of the variables (4.44) we get the following quasi-static problem to leading order,

$$\frac{R_t}{R} y_q = \frac{1}{R^4 \delta_1^3} y_{qqq}, \quad -\infty < q < \infty, \tag{4.45}$$

$$y(0^+,t) = y(0^-,t), \tag{4.46}$$

$$y_q(0^+,t) - y_q(0^-,t) = 1, \tag{4.47}$$

$$y_{qq}(0^+,t) = y_{qq}(0^-,t), \tag{4.48}$$

$$y_{qqq}(0^+,t) = y_{qqq}(0^-,t), \tag{4.49}$$

where

$$u^*(t)/L = 1, \quad r_u^*(t) = -\frac{m}{2}[y_q(0^+,t) + y_q(0^-,t)],$$

$$R_t = \left[\frac{r_u^*}{u^*} - \frac{1}{R}\right]. \tag{4.50}$$

The far-field conditions have not been included in the problem for the inner solution, as the far-field conditions should be employed in the solution of the outer problems, which will later influence the inner solution during the matching process. Note that in (4.45)–(4.50), the governing equation for the evolution of $y(q,t)$ can be seen to be quasi-static, with the time variation dictated by $R_t(t)$ as prescribed in (4.50). Due to the possible appearance of early transients before the quasi-static description becomes relevant, initial conditions have not been explicitly included in (4.45)–(4.50).

Since we expect the grain located at the origin to be shrinking, we shall assume that $w(t) := \delta_1^3 R^3 R_t = \delta_1^3 R^3 [r_u^*/u^* - 1/R] < 0$. We may also expect the outer solutions to be bounded (given in terms of the original variables). With this in mind, we find that the solution to (4.45)–(4.50) is

$$y(q) = C + e^{-\gamma q/2}\left[\frac{1}{3\gamma}\cos\left(\sqrt{3}\gamma q/2\right) - \frac{1}{\sqrt{3}\gamma}\sin\left(\sqrt{3}\gamma q/2\right)\right] \quad q > 0, \tag{4.51}$$

$$y(q) = C + \frac{1}{3\gamma} e^{\gamma q}, \quad q < 0, \tag{4.52}$$

where $\gamma = w^{1/3}$ and C is a constant to be determined by matching with the solution to the outer problems. From (4.51), (4.52) and (4.43), we obtain that $r_u^*(t) = m/6$. Similarly, we get from (4.43) and (4.44), noting that δ_2 is small, that to leading order $u^*(t) = L$. Using these approximations in (4.37), we now find that to leading order

$$R_t = \left[\frac{m}{6L} - \frac{1}{R}\right], \tag{4.53}$$

which corresponds to Eq. (1.1) with $r_u^*/u^* = m/6L$, as discussed in the Section 1 (see Figs. 7 and 8). A fuller description of the solution and how the inner solution matches with the outer solutions will be given elsewhere [16].

5. Discussion and conclusions

Our results show that in a thin film, grain growth is strongly affected by the exterior surfaces. This differs from the results of the analysis for a single shrinking grain attached to one external surface in a 3-D geometry [15], where the kinetics were almost unaffected by the surface. We found that the exterior surface does not allow the formation of a stationary catenoidally shaped grain boundary which stops the grain boundary migration, as suggested by Mullins [5] and which served as the basis for the simulations in Ref. [6]. Nevertheless, Mullins' perspective [5] helps in understanding our results. In our geometry there are two special shapes for the grain boundary. One is catenoidal, which is stationary if it can be realized, since the principle

curvatures are in different directions and their net effect balances out. The second is a cylindrically shaped grain boundary, where one component of the mean curvature vanishes and the other component drives the grain boundary migration; this corresponds to a freely moving grain boundary whose velocity is apparently maximal, except for the motion of the grain boundary just prior to annihilation when both principle curvatures are in the same direction and acceleration occurs.

The catch is that neither of these special shapes can be precisely achieved when $0 < m < 2$, since the former requires that the groove serve an anchor for grain boundary and the latter requires that $m = 0$. If $0 < m \ll 1$, the inclination of the grain boundary, r_u, is small, and thus the grain shape should be close in some sense to that of a "freely moving" grain boundary. By looking at Eq. (4.53), we see that if the radius of the grain boundary is much larger than the film thickness, the in-plane component of the curvature becomes important and the relative effect of the $1/r$ component decreases. We found that while the grain boundary and grain groove remain mobile, delay in the grain boundary migration can allow the groove root to grow and lead to voiding. The competition between two trends: shrinking of the grain and growth of the groove, gives rise to an annihilation–break-up transition which can be expressed in terms of a critical value, $R^* = R^*(L, m)$, of the initial radius of the embedded grain, as indicated in Fig. 2. The value $R^* = R^*(L, m)$ can be interpreted as a generalization of the notion of critical curvature employed in the simulations in Ref. [6]. While for $L \gg 1, R^*$ depend linearly on L, when $L \approx 0.1 - 0.5$ or smaller, R^* is seen to depend nonlinearly on L; this change in the nature of the annihilation–break-up transition occurs at nanoscale film thicknesses.

Note that our asymptotic analysis also predicts a transition between the two trends. When the (dimensionless) parameters m and L/R_0 are small, then to leading order the equations of motion can be written as a PDE for the exterior surface coupled with an ODE for grain boundary motion, and the grain boundary shape is predicted to be parabolic. In order to understand when the transition occurs it is necessary to distinguish between the relative size of the two small parameters. When $mR_0/L = \mathcal{O}(1)$, i.e. the two small parameters are comparable in size, then a radial variant of Mullins' equation of motion for thermal grooving is predicted and break-up can be expected to occur. If $mR_0/L \ll 1$, or stated more precisely, if $mR_0/L = \mathcal{O}(m^\alpha)$ with $0 < \alpha < 1$, then to leading order, the shape of the exterior surface near the groove root should be quasi-static, with the velocity of the groove root dictated by (1.1).

Our numerics indicate further that the rate of groove growth in the moving grain boundary is greatly delayed relative to the rate of the groove growth in stationary grain grooves. We may estimate pinch-off time by $t_{\text{pinch-off}} \approx (\sqrt{2}\Gamma(5/4)L/m)^4$, the time to pinch-off for a flat stationary grain boundary [12, Eq. 30]. Noting that $\Gamma(5/4) \approx 0.91$, this yields the estimates $t_{\text{pinch-off}} \approx 105.5$ when $m = 0.1$, $L = 0.25$, and $t_{\text{pinch-off}} \approx 2.7 \times 10^4$ when $m = 0.1, L = 1$. These estimates fall far short of our numerical results; in Fig. 2 the time to break-up can be seen to be about 1761 when $m = 0.1, L = 0.25$, and in Fig. 3 the time to break-up can be seen to be about 8×10^5 when $m = 0.1$, $L = 1.0$. The simulations show acceleration in the shrinkage of the grain just prior to annihilation, as has been observed experimentally [7,18].

Our results can be applied to the "wedge-shaped geometry" investigated experimentally by Rath and Hu [19]. We believe that the anomalously slow rate of grain boundary motion in Al observed in Ref. [19] can be explained in terms of the effect of the exterior surface and surface grooving during grain boundary motion as we saw in our simulations. Rath and Hu [19] remarked that they observed grain grooving in their experiments. This is of interest, as elsewhere, see e.g. Ref. [4] and references therein, grooving had not been seen to occur in Al due to an oxidation layer on the exterior surface. We cannot confirm the explanation given in Ref. [20] that the slow dynamics observed in Ref. [19] were caused by jerky motion, as we did not see any indication of jerky motion in our simulations.

Ideally we should like to generalize our results to a true polycrystalline setting. Were we to look at a segment of a groove root line lying on the exterior surface of a thin film from above, then by interpreting $R(t)$ as the locally defined in plane curvature of the groove root, (1.1) and (4.53) can be used to prescribe the locally defined in-plane velocity. Nevertheless, to complete the description of the motion of an array of groove roots, it is necessary to understand the quadruple junctions which form where groove roots meet and intersect along the exterior surface and accompanying phenomena such as pitting [10,9]; this step lies beyond the scope of the present analysis.

It is a happy coincidence that, on one hand, since the dimensions of the nanofilm system are on the order of about 10 nm, or in other words, about 100 interatomic distances, continuum models can be realistically implemented for describing nanofilm systems, and on the other hand, voiding in thin films takes place on a laboratory time scale. This allows the annihilation–break-up transition both to be successfully modeled with continuum models and to be realized experimentally on a laboratory time scale. Note that for thicker films, a continuum model would be justified, but the transition would be become difficult to explore experimentally.

Acknowledgements

The authors would like to thank Isaac Goldhirsch for his questions and comments. We would like to acknowledge the support of the Japan Technion Society Research Fund.

Appendix A

Claim. There do not exist steady-state solutions to the system (2.2)–(2.13).

Proof of the claim. Suppose there did exist steady-state solutions to (2.2)–(2.13). Then setting $h_t = 0$ in (2.3), and noting (2.10), (2.11), we get

$$\frac{rk_r}{\sqrt{1+h_r^2}} = 0.$$

The boundary conditions (2.9), (2.13) imply that

$$k = 0, \quad 0 < r < \infty, \quad r \neq R(t). \tag{6.53}$$

By considering (2.4) and (2.11), we get that

$$\frac{rh_r}{\sqrt{1+h_r^2}} = 0, \quad 0 < r < R(t),$$

and hence

$$h = c_1 \ (= \text{constant}), \quad 0 < r < R(t). \tag{6.54}$$

By (6.53) and (2.4), it follows that

$$\frac{rh_r}{\sqrt{1+h_r^2}} = c_2 \ (= \text{constant}), \quad R(t) < r < \infty,$$

whence

$$h_r = \frac{c_2}{\sqrt{r^2 - c_2^2}}. \tag{6.55}$$

However, (6.55) has only unbounded solutions which cannot satisfy (2.13), unless $c_2 = 0$. Thus setting $c_2 = 0$, (6.55) and (2.6) imply that

$$h = c_1, \quad 0 < r < \infty. \tag{6.56}$$

Note that (6.56) contradicts (2.7) unless $m = 0$. To obtain a contradiction also when $m = 0$, we continue as follows. Setting $r_t = 0$ in (2.2) and noting (2.8), (2.12),

$$\frac{r_{uu}}{1+r_u^2} - \frac{1}{r} = 0, \quad 0 < u < u^*, \quad r_u(0) = r_u(u^*) = 0. \tag{6.57}$$

However, the equation in (6.57) implies that $r_{uu} > 0$ which in conjunction with $r_u(0) = 0$ yields that $r_u(u^*) > 0$, which contradicts the second boundary condition in (6.57). □

References

[1] Kanel J, Novick-Cohen A, Vilenkin A. Acta Mater 2003;51:1981.
[2] Kanel J, Novick-Cohen A, Vilenkin A. Defect and Diffusion Forum 2002;216–2:299.
[3] Min D, Wong H. Acta Mater 2002;50:5155.
[4] Barmak K, Kim J, Archibald WE, Rohrer GS, Rollet AD, Kinderlehrer D, et al. Scripta Mater 2006;54:1059.
[5] Mullins WW. Acta Metall 1958;6:414.
[6] Frost H, Thompson C, Walton D. Acta Mater 1990;38(8):6397.
[7] Palmer MA, Glicksman ME, Rajan K. Acta Mater 1998;46(18):6397.
[8] Wong H, Voorhees MJ, Miksis MJ, Davis SH. JAP 1997;81:6091.
[9] Srolovitz, Safran. JAP 1986;60:255.
[10] Genin F, Mullins W, Wynblatt P. Acta Metall 1992;40(12):3239.
[11] Saxena R, Frederick MJ, Ramanat J, Gill WN, Plawsky JL. Phys Rev B 2005;72:115425-1–6.
[12] Mullins WW. J Appl Phys 1957;28:333.
[13] Vilenkin A, Kris R, Brokman A. J Appl Phys 1997;81:238.
[14] Bouville M, Chi DZ, Srolovitz DJ. Phys Rev Lett 2007;98(085503-1).
[15] Kanel J, Novick-Cohen A, Vilenkin A. Acta Mater 2006;54:2589.
[16] Zelekman-Smirin O. PhD. Thesis, Technion-IIT, in progress.
[17] Dunn C. Acta Metall 1966;14:221.
[18] Thon A, Brokman A. J Appl Phys 1988;63:5331.
[19] Rath B, Hu H. Trans Am Inst Min Eng 1969;245:1577.
[20] Gottstein G, Shvindlerman L. Scripta Metall 1992;27:1521.